Semicond. Sci. Technol. **23** (2008) 125008 (5pp) doi:10.1088/0268-1242/23/12/125008

Electronic states in quantum rings based on narrow-gap III–V semiconductors

C González-Santander and F Domínguez-Adame

GISC, Departamento de Física de Materiales, Universidad Complutense, E-28040 Madrid, Spain

E-mail: cglezsantander@fis.ucm.es

Received 27 May 2008, in final form 4 September 2008
Published 21 October 2008
Online at stacks.iop.org/SST/23/125008

Abstract

We report the theoretical electronic structure of two-dimensional quantum rings based on narrow-gap III–V semiconductors, subjected to a strong perpendicular magnetic field. The electron dynamics is considered within the framework of the envelope-function approximation in a two-band model. A finite width of the quantum ring is taken into account. The resulting envelope functions and energy spectrum are found by solving exactly the corresponding (Dirac-like) wave equation. As a working example, we consider the InP–$In_{0.53}Ga_{0.47}As$–InP quantum rings and discuss in detail our results in this system. The obtained levels are compared to the one-band model (Schrödinger-like) predictions. We find that both approaches may differ significantly, especially in the case of strong magnetic fields.

1. Introduction

Quantum rings (QRs) have been investigated due to their physical properties as well as for their potential applications in nanoelectronics [1–10]. QRs are small semiconductor ring-shaped structures in which electrons are confined in all spatial dimensions. As a consequence, discreteness of energy and charge arises, as in atomic systems. Their physical properties can be continuously tuned by changing the geometry and the applied external potentials, making them ideal candidates for applications in future devices.

The electronic structure of QRs can be obtained within the envelope-function approximation [11, 12], the system being usually described by a scalar Hamiltonian (Schrödinger-like) corresponding to decoupled bands. Spatial confinement of carriers arises from the band-edge offset of the semiconductors forming the QR [4, 5, 8–10]. Following this approach, Bandos *et al* studied the optical transitions in two-dimensional (2D) QRs under a strong perpendicular magnetic field [8]. They considered finite-width QRs based on wide-gap semiconductors, solving analytically the corresponding effective-mass equation for a single envelope function. However, this approach cannot adequately describe those QRs whose band offset is comparable to the magnitude of the gap, and a more realistic model is required to properly describe the band structure.

In this work we calculate the envelope functions and energy levels of 2D QRs under an applied magnetic field within a two-band model, assuming perfect axial symmetry of the nanostructures. This approach is known to be valid in a large variety of semiconductors where the coupling of the bands is not negligible, as occurs in some narrow-gap III–V semiconductors [13, 14]. We solve analytically the Dirac-like equation for the two coupled envelope functions, one corresponding to the conduction band (s-like) and the other to the valence band (p-like). Results are compared to the one-band model (Schrödinger-like) predictions. As a major conclusion we claim that both approaches may differ significantly, especially at high magnetic fields.

2. Model of QRs

The system we study in this work is a 2D QR of inner and outer radii R_1 and R_2, respectively, made of two different narrow-gap III–V semiconductors. Because of the offset between the conduction and valence bands at the interfaces, carriers can be confined at the QR, namely between R_1 and R_2. For simplicity, we deal only with low-doping levels and the band bending can be safely neglected hereafter. We treat the resulting electronic structure by means of the $\boldsymbol{k}\cdot\boldsymbol{p}$ approximation. The electronic wavefunction is written as a sum of products of band-edge Bloch functions with slowly varying envelope functions. To proceed, let E_g^{in} and E_g^{out} be the gaps of the semiconductors inside and outside the QR. Let us denote the relative offset of the gap centres by V (in what follows we take the centre of the gap in the QR as the origin of

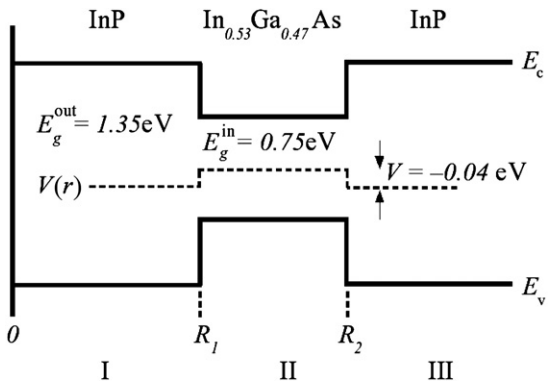

Figure 1. A schematic band-edge diagram along the radial direction of a InP–$In_{0.53}Ga_{0.47}As$–InP 2D QR.

energies). As an example, the band-edge alignment along the radial direction for a InP–$In_{0.53}Ga_{0.47}As$–InP 2D QR is shown in figure 1.

As pointed out earlier, we restrict ourselves to two nearby bands. Consequently, there are two coupled envelope functions satisfying an effective 2×2 Dirac-like equation. In addition, we will consider a uniform magnetic field applied perpendicular to the QR plane, deriving from the vector potential $\boldsymbol{A} = (1/2)\boldsymbol{B} \times \boldsymbol{r}$. Assuming that both the gap and the gap centre depend only on the radial coordinate r, the resulting equation can be written as

$$\left[v\boldsymbol{\alpha} \cdot (\boldsymbol{p} - e\boldsymbol{A}) + \tfrac{1}{2}E_g(r)\beta + V(r)\right]\chi(r,\theta) = E\chi(r,\theta), \quad (1)$$

where $\chi(r,\theta)$ is a two-component spinor. Here $E_g(r)$ is the position-dependent gap and $V(r)$ gives the energy of the gap centre. The velocity parameter v is related to Kane's momentum matrix elements and is given by $v^2 = E_g/2m^*$. In spite of the fact that both E_g and the effective mass m^* are position-dependent, the value of v is almost constant in direct-gap III–V semiconductors [13].

Equation (1) describes a model system of a symmetric two-band semiconductor, and it is the basis for a more elaborate analysis [15]. We take into account the magnetic field effects through a minimal coupling in the envelope-function Hamiltonian [16]. A detailed discussion of the effects of magnetic fields in a multiband $\boldsymbol{k}\cdot\boldsymbol{p}$ approach can be found in [17], where it is shown that these effects enter the Hamiltonian in a way similar to the one-band effective-mass equation. Hereafter we keep the minimal two-band model since it can be analytically solved while providing a reasonable description of the electronic states.

3. Envelope functions and energy levels

We use the following representation of the 2×2 Dirac matrices, $\alpha_x = \sigma_1, \alpha_y = \sigma_2$ and $\beta = \sigma_3, \sigma_i$ being the Pauli matrices. Due to the axial symmetry of the Dirac-like equation (1), the spinor can be factorized in the polar coordinates as follows [18]:

$$\chi(r,\theta) = \frac{1}{\sqrt{2\pi r}}\begin{pmatrix} \mathrm{e}^{\mathrm{i}(\kappa-1/2)\theta}F(r) \\ \mathrm{i}\,\mathrm{e}^{\mathrm{i}(\kappa+1/2)\theta}G(r)\end{pmatrix}, \quad (2)$$

where $\kappa = \pm\frac{1}{2}, \pm\frac{3}{2}, \ldots$ and the total angular momentum is $j = \kappa \pm \frac{1}{2}$. Inserting (2) into (1) we can obtain the following set of coupled differential equations for the upper and lower components [18]:

$$\left(\frac{\mathrm{d}}{\mathrm{d}r} + \frac{\kappa}{r} - \frac{eBr}{2}\right)G(r) = \frac{1}{\hbar v}\left[E - V(r) - \frac{1}{2}E_g(r)\right]F(r), \quad (3a)$$

$$\left(-\frac{\mathrm{d}}{\mathrm{d}r} + \frac{\kappa}{r} - \frac{eBr}{2}\right)F(r) = \frac{1}{\hbar v}\left[E - V(r) + \frac{1}{2}E_g(r)\right]G(r). \quad (3b)$$

We now scale the radial coordinate by introducing the variable $z = r/l_m$, where $l_m = \sqrt{\hbar/eB}$ is the magnetic length. Thus, the above equations can be recast in the dimensionless form

$$\left(\frac{\mathrm{d}}{\mathrm{d}z} + \frac{\kappa}{z} - \frac{z}{2}\right)G(z) = [\epsilon - \alpha^+(z)]F(z), \quad (4a)$$

$$\left(-\frac{\mathrm{d}}{\mathrm{d}z} + \frac{\kappa}{z} - \frac{z}{2}\right)F(z) = [\epsilon - \alpha^-(z)]G(z), \quad (4b)$$

where for brevity we have defined $\epsilon = l_m E/\hbar v$ and $\alpha^{\pm}(z) = (l_m/\hbar v)[V(z) \pm E_g(z)/2]$. Note that the functions $\alpha^{\pm}(z)$ are piecewise constant along the radial direction. We now look for the solution of the coupled equations on each interval, hereafter labelled I ($0 < z < z_1$), II ($z_1 < z < z_2$) and III ($z > z_2$), with $z_i = R_i/l_m$ (see figure 1). To this end, we insert (4*b*) into (4*a*) to obtain

$$\left[\frac{\mathrm{d}^2}{\mathrm{d}z^2} - \frac{\kappa(\kappa-1)}{z^2} - \frac{z^2}{4} + \left(\kappa + \frac{1}{2}\right) + \eta(z)\right]F(z) = 0, \quad (5)$$

with $\eta(z) = [\epsilon - \alpha^+(z)][\epsilon - \alpha^-(z)]$.

It is not difficult to express the solution of (5) on each interval in terms of the confluent hypergeometric functions [19]

$$F_\nu(z) = z^m\,\mathrm{e}^{-z^2/4}\left[C_\nu^M M(a_\nu, b, z^2/2) + C_\nu^U U(a_\nu, b, z^2/2)\right], \quad (6a)$$

where the index ν = I, II, III refers to each interval, and C_ν^M and C_ν^U are integration constants to be determined from the boundary conditions. The definition of the various parameters appearing in (6*a*) depends on the sign of the quantum number κ. Thus, for $\kappa > 0$ one finds $m = \kappa, a_\nu = -\eta_\nu/2$ and $b = \kappa + 1/2$. On the other hand, for $\kappa < 0$ we have $m = 1 - \kappa, a_\nu = -\eta_\nu/2 - \kappa + 1/2$ and $b = -\kappa + 3/2$. Here η_ν refers to the value of the function $\eta(z)$ defined above on each interval. Finally, using (4*b*) we get

$$G_\nu(z) = -z^{m+1}\,\mathrm{e}^{-z^2/4}\left(\frac{a_\nu}{\epsilon - \alpha_\nu^-}\right)\left[\frac{C_\nu^M}{b}M(1+a_\nu, 1+b, z^2/2) - C_\nu^U U(1+a_\nu, 1+b, z^2/2)\right]. \quad (6b)$$

Since the functions $M(a_\nu, b, z^2/2)$ and $U(a_\nu, b, z^2/2)$ diverge for $z \to \infty$ and $z \to 0$, respectively, the normalization condition of the envelope function

$$\int_0^\infty \mathrm{d}z[|F(z)|^2 + |G(z)|^2] < \infty$$

implies $C_{\mathrm{I}}^U = C_{\mathrm{III}}^M = 0$, leaving four unknown integration constants. Moreover, the two envelope functions are continuous at the heterojunctions ($z = z_1$ and $z = z_2$), thus providing four equations for the remaining integration constants. The secular equation to obtain the energy levels is then written as follows:

$$\begin{vmatrix} D_{11} & D_{12} & D_{13} & 0 \\ D_{21} & D_{22} & D_{23} & 0 \\ 0 & D_{32} & D_{33} & D_{34} \\ 0 & D_{42} & D_{43} & D_{44} \end{vmatrix} = 0. \tag{7}$$

For brevity we have introduced the notation

$$\begin{aligned}
D_{11} &= M\left(a_{\mathrm{out}}, b, z_1^2/2\right), \\
D_{12} &= -M\left(a_{\mathrm{in}}, b, z_1^2/2\right), \\
D_{13} &= -U\left(a_{\mathrm{in}}, b, z_1^2/2\right), \\
D_{21} &= \frac{\lambda_{\mathrm{out}}}{b} M\left(1 + a_{\mathrm{out}}, 1 + b, z_1^2/2\right), \\
D_{22} &= -\frac{\lambda_{\mathrm{in}}}{b} M\left(1 + a_{\mathrm{in}}, 1 + b, z_1^2/2\right), \\
D_{23} &= \lambda_{\mathrm{in}} U\left(1 + a_{\mathrm{in}}, 1 + b, z_1^2/2\right), \\
D_{32} &= M\left(a_{\mathrm{in}}, b, z_2^2/2\right), \\
D_{33} &= U\left(a_{\mathrm{in}}, b, z_2^2/2\right), \\
D_{34} &= -U\left(a_{\mathrm{out}}, b, z_2^2/2\right), \\
D_{42} &= -\frac{\lambda_{\mathrm{in}}}{b} M\left(1 + a_{\mathrm{in}}, 1 + b, z_2^2/2\right), \\
D_{43} &= \lambda_{\mathrm{in}} U\left(1 + a_{\mathrm{in}}, 1 + b, z_2^2/2\right), \\
D_{44} &= -\lambda_{\mathrm{out}} U\left(1 + a_{\mathrm{out}}, 1 + b, z_2^2/2\right),
\end{aligned}$$

with $\lambda_\mu = a_\mu / \left(\epsilon - \alpha_\mu^-\right)$. The subscripts $\mu = \mathrm{in}, \mathrm{out}$ refer to the value of the corresponding parameter inside and outside the quantum well, respectively.

4. Numerical results

We have solved numerically the secular equation (7) for a 2D QR made of InP–$In_{0.53}Ga_{0.47}As$–InP. These two semiconductors present nearly equal Kane matrix elements, leading to $\hbar v \sim 0.77$ eV nm. The energy gaps are $E_g^{\mathrm{in}} = 0.75$ eV and $E_g^{\mathrm{out}} = 1.35$ eV, and the offset of the band centre is $V = -0.04$ eV (see figure 1). The inner and outer radii are set $R_1 = 10$ nm and $R_2 = 20$ nm, respectively. The magnetic length is given by $l_m = (26/\sqrt{B})$ nm, where B is expressed in Tesla.

Using the above set of parameters, we first obtain the envelope functions in the conduction and valence bands. Figure 2 shows the envelope functions $F(r)$ and $G(r)$ of the ground and first excited states in the conduction and valence bands for $\kappa = \frac{1}{2}$ when the applied magnetic field is $B = 0.1$ T. Note that the amplitude of the smaller component of the spinor ($G(r)$ for states in the conduction band and $F(r)$ for states in the valence band) becomes comparable to the amplitude of the larger component in the case of the excited states. This points out the relevance of the non-parabolicity effects for states far from the band edge, as expected.

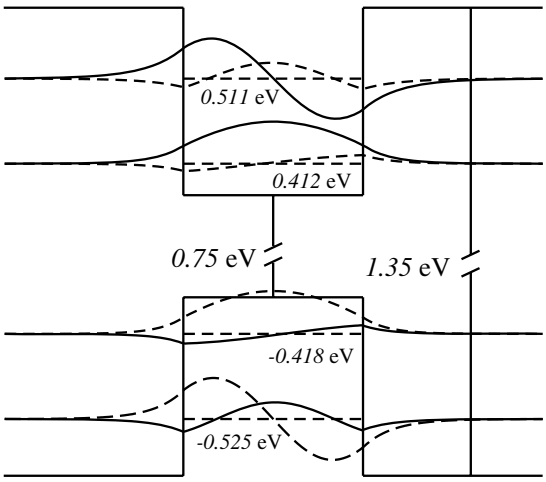

Figure 2. Envelope functions $F(r)$ (solid lines) and $G(r)$ (dashed lines) of the ground and first excited states in the conduction and valence bands for $\kappa = \frac{1}{2}$ when the applied magnetic field is $B = 0.1$ T. The energy of the level is also indicated in the plot.

In order to get a quantitative estimation of the relevance of the lower component, we have calculated the magnitude

$$\frac{I_G}{I_F} = \frac{\int_0^\infty \mathrm{d}r |G(r)|^2}{\int_0^\infty \mathrm{d}r |F(r)|^2}. \tag{8}$$

In the one-band approximation for states in the conduction band, the smaller component $G(r)$ is neglected and this ratio vanishes. Therefore, the larger the ratio the larger the contribution of the $G(r)$ component. Similar comments can be stated for the inverse I_F/I_G concerning the states in the valence band. Figure 3 shows the envelope functions of the states in the conduction and valence bands with $\kappa = \frac{1}{2}$ and different values of the magnetic fields. Remarkably, only the smaller component is greatly affected on increasing the magnetic field ($G(r)$ for conduction band states and $F(r)$ for valence band states). The ratios I_G/I_F for conduction band states and I_F/I_G for valence band states are nonvanishing and increase upon increasing the magnetic field. Therefore, we come to the conclusion that the two-band model is required to get an accurate description of the electronic states in the QR, especially at high magnetic fields.

Furthermore, we studied the electronic levels in the conduction and valence bands as a function of the applied magnetic field, for different values of the quantum number κ. Results are shown in figure 4, where energy is measured from the centre of the gap in the $In_{0.53}Ga_{0.47}As$ quantum well. At low magnetic field the energy levels depend quadratically on B while at very high magnetic field the dependence is linear. Similar trends were found in 2D QRs within the one-band approximation (see figure 1 in [8]). Note that the state with lowest energy in the conduction band always presents a positive value of the quantum number κ. Nevertheless, at the crossing points (marked by circles in figure 4), the minimum

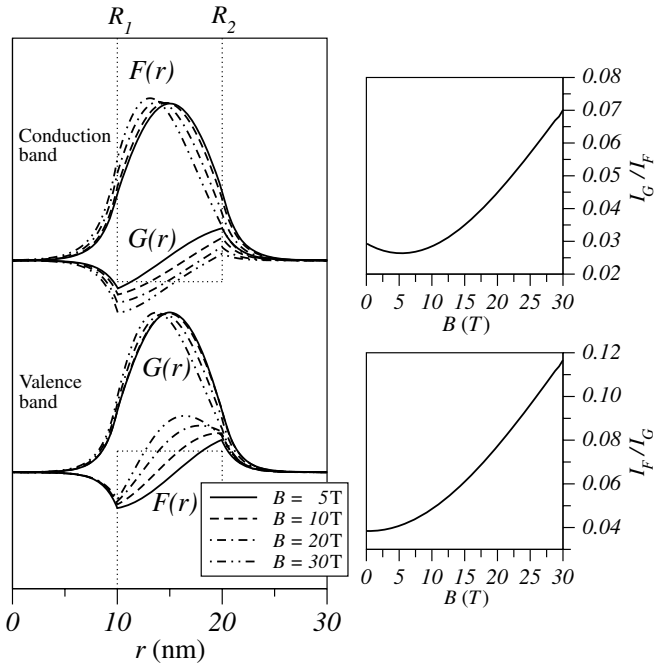

Figure 3. Envelope functions $F(r)$ and $G(r)$ of the states in the conduction (upper panel) and valence (lower panel) bands with $\kappa = \frac{1}{2}$ for different values of the magnetic fields. The right panels show the ratios I_G/I_F and I_F/I_G for the conduction and valence band states, respectively, as a function of the applied magnetic field.

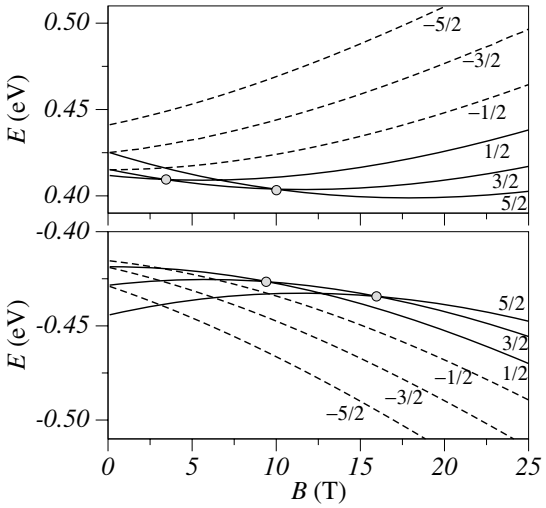

Figure 4. Electronic levels in the conduction and valence bands (upper and lower panels, respectively) as a function of the applied magnetic field, for different values of the quantum number κ indicated on each curve.

energy is reached at a higher value of the quantum number κ. In contrast, states with negative κ never cross and their energy increases on increasing $|\kappa|$ for any given magnetic field. Analogous behaviour is observed in the valence band states.

The different behaviour of positive and negative κ states shown above also manifests in the energy separation ΔE between the two lowest states with the same value of the quantum number κ. Figure 5 displays this difference for

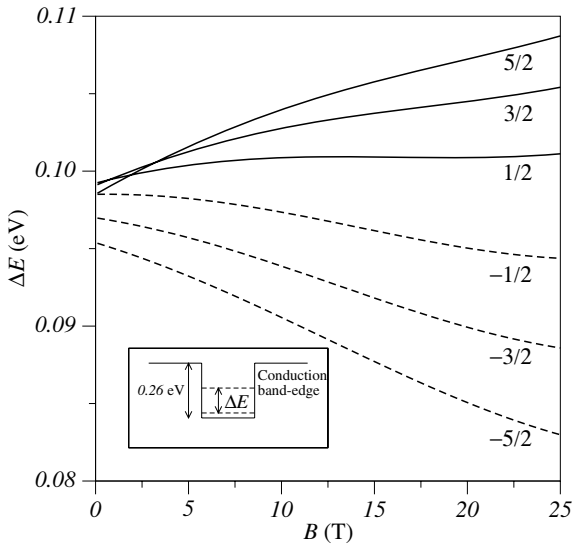

Figure 5. Energy difference between the two lowest states in the conduction band as a function of the applied magnetic field, for various values of the quantum number κ indicated on each curve.

states in the conduction band as a function of the magnetic field. Remarkably, the difference increases (decreases) for positive (negative) values of κ on increasing the strength of the magnetic field.

5. Comparison to the one-band approach

Let us now discuss the limit of wide-gap semiconductors within the two-band approach. For the sake of concreteness, we restrict ourselves to the conduction band states and positive κ, although other cases can be handled in a similar fashion. To proceed we define $\widetilde{E} = E - E_g^{\rm in}/2$, namely $\widetilde{E}$ is nothing but the energy level referred to the bottom of the quantum well. Therefore we can rewrite

$$\eta_{\rm in} = \left(\frac{l_m}{\hbar v}\right)^2 \widetilde{E}\left(\widetilde{E} + \frac{1}{2}E_g^{\rm in}\right),$$
$$\eta_{\rm out} = -\left(\frac{l_m}{\hbar v}\right)^2 (\Delta E_c - \widetilde{E})\left(\frac{1}{2}E_g^{\rm out} - \Delta E_C + \widetilde{E}\right), \tag{9}$$

where ΔE_c is the conduction band offset. The wide-gap approximation assumes that $\widetilde{E} \ll E_g^{\rm in}/2$ and, consequently, $\widetilde{E} \ll E_g^{\rm out}/2$. In this situation one gets $\eta_{\rm in} \simeq 2\widetilde{E}/\hbar\omega_c$ and $\eta_{\rm out} \simeq -2(\Delta E_c - \widetilde{E})/\hbar\omega_c$, where $\omega_c = eB/m^*$, assuming the same effective mass m^* in the barrier and the quantum well. Finally, replacing the quantum number κ by $\ell + \frac{1}{2}$, ℓ being the angular momentum, it is straightforward to check that the secular equation (7) reduces to that obtained in [8] within the one-band framework.

To get a quantitative comparison of both approaches, we have calculated the energy difference, $\Delta E_{\rm cv}$, between the lowest state in the conduction band and the highest state in the valence band as a function of the applied magnetic field, as shown in figure 6. Both results are rather different on increasing the magnetic field, indicating again the failure of the one-band approximation at high magnetic fields. We observe

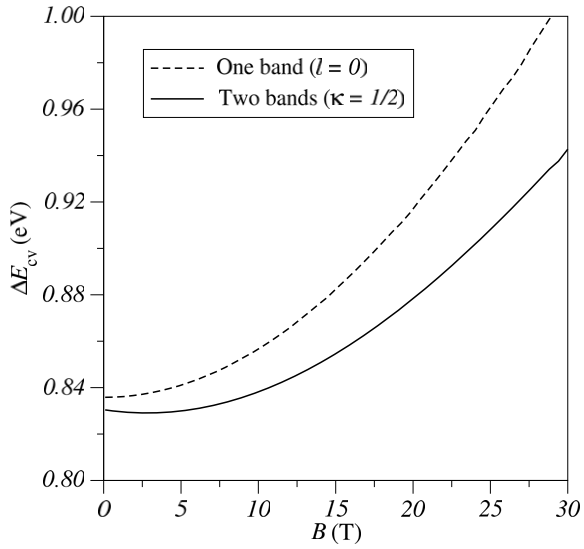

Figure 6. Energy difference between the lowest state in the conduction band and the highest state in the valence band as a function of the applied magnetic field. Curves correspond to calculations within the one-band ($\ell = 0$, dashed line) and two-band ($\kappa = \frac{1}{2}$, solid line) frameworks.

that the magnitude of this energy difference is always smaller within the two-band approximation. The observed *shrinkage* of the electronic spectrum seems to be a universal property of Dirac-like equations, as was formerly observed in Dirac–Kroning–Penney models and sawtooth superlattices based on narrow-gap III–V semiconductors (see [20] for further details).

6. Summary

We have studied theoretically the electronic states of 2D QRs made of narrow-gap III–V semiconductors, whose electron dynamics is described by means of an effective Dirac-like equation within the framework of an effective-mass $\boldsymbol{k} \cdot \boldsymbol{p}$ approximation. The effects of an external magnetic field applied perpendicularly to the 2D electron gas were also taken into account. Band-edge offsets give rise to the confining potential for carriers in QRs based on semiconductor heterostructures, such as those studied in this work. As a working example we consider InP–$In_{0.53}Ga_{0.47}As$–InP QRs and discuss in detail our results in this system. We found that the carriers remain localized in the potential well for the system parameters considered here.

Remarkably, the smaller component of the envelope function is strongly affected by the magnetic field. Results have been compared to the one-band model (Schrödinger-like) predictions, when the role of the small component is neglected. The relevance of the smaller component is higher at large values of the applied magnetic field (see insets of figure 3). In addition, we have also found shrinkage of the electronic spectrum within the two-band model framework, as compared to the predictions of the one-band approach. The shrinkage is again more important at a high magnetic field (see figure 6). Therefore, we come to the conclusion that the one-band approach overestimates the energy levels of the QRs based on narrow-gap semiconductors, and a two-band model is required to get a more accurate electronic structure, especially in the case of strong magnetic fields currently available in the laboratory.

Finally, some words concerning Coulomb-induced electron–hole correlations are in order. The present calculation neglects the electron–hole interaction, which is likely to be important in realistic QRs. Using the correspondence between the two-band model and relativistic quantum mechanics, we can conclude that the binding energy of the electron–hole pair is larger than the one-band prediction [21]. In other words, the electron–hole interaction also experiences the shrinkage of the spectrum mentioned above. Therefore, the depression of levels predicted with the single particle approach would be even larger when the electron–hole interaction is taken into account.

Acknowledgments

This work was supported by MEC (Project MOSAICO) and BSCH-UCM (Project PR34/07-15916). The authors thank M Amado and J Cuesta for helpful conversations.

References

[1] Barticevic Z, Pacheco M and Latgé A 2000 *Phys. Rev.* B **62** 6963
[2] Lorke A, Luyken R J, García J M and Petroff P M 2001 *Jpn. J. Appl. Phys.* **40** 1857
[3] Song J and Ulloa S E 2001 *Phys. Rev.* B **63** 125302
[4] Planelles J, Jaskólski W and Aliaga J I 2001 *Phys. Rev.* B **65** 033306
[5] Voskoboynikov O, Li Y, Lu H-M, Shih C-F and Lee C P 2002 *Phys. Rev.* B **66** 155306
[6] Blossey R and Lorke A 2002 *Phys. Rev.* E **65** 021603
[7] Granados D and García J M 2003 *Appl. Phys. Lett.* **82** 2401
[8] Bandos T V, Cantarero A and García-Cristóbal A 2006 *Eur. Phys. J.* B **53** 99
[9] Filikhin I, Suslov V M and Vlahovic B 2006 *Phys. Rev.* B **73** 205332
[10] Amado M, Lima R P A, González-Santander C and Domínguez-Adame F 2007 *Phys. Rev.* B **76** 073312
[11] Bastard G 1981 *Phys. Rev.* B **24** 5693
[12] Bastard G 1989 *Phys. Rev.* B **40** 6420
[13] Beresford R 1993 *Semicond. Sci. Technol.* **8** 1957
[14] Domínguez-Adame F, Maciá E, Méndez B, Roy C L and Khan A 1995 *Semicond. Sci. Technol.* **10** 797
[15] Beresford R 1994 *Phys. Rev.* B **49** 13663
[16] Agassi D 1994 *Phys. Rev.* B **49** 10393
[17] Planelles J and Jaskólski W 2003 *J. Phys.: Condens. Matter* **15** L67
[18] Villalba V M and Rincón Maggiolo A 2001 *Eur. Phys. J.* B **22** 31
[19] Abramowitz M and Stegun I A 1972 *Handbook of Mathematical Functions* (New York: Dover)
[20] Domínguez-Adame F and Méndez B 1994 *Semicond. Sci. Technol.* **9** 1358
[21] Greiner W 2000 *Relativistic Quantum Mechanics* (Berlin: Springer)